NANO LETTERS

Letter

pubs.acs.org/NanoLett

Self-Powered, One-Stop, and Multifunctional Implantable Triboelectric Active Sensor for Real-Time Biomedical Monitoring

Ye Ma,[†] Qiang Zheng,[‡] Yang Liu,[†] Bojin Shi,[‡] Xiang Xue,[†] Weiping Ji,[†] Zhuo Liu,[§] Yiming Jin,[‡] Yang Zou,[§] Zhao An,[†] Wei Zhang,[†] Xinxin Wang,[‡] Wen Jiang,[‡] Zhiyun Xu,[†] Zhong Lin Wang,[*,‡,∥] Zhou Li,[*,‡] and Hao Zhang[*,†]

[†]Institute of Cardiothoracic Surgery at Changhai Hospital, Second Military Medical University, Shanghai 200433, PR China

[‡]Beijing Institute of Nanoenergy and Nanosystems, Chinese Academy of Science, Beijing 100083, PR China

[§]School of Biological Science and Medical Engineering, Beihang University, Beijing 100191, PR China

[∥]School of Materials Science and Engineering, Georgia Institute of Technology, Atlanta, Georgia 30332, United States

Supporting Information

ABSTRACT: Operation time of implantable electronic devices is largely constrained by the lifetime of batteries, which have to be replaced periodically by surgical procedures once exhausted, causing physical and mental suffering to patients and increasing healthcare costs. Besides the efficient scavenging of the mechanical energy of internal organs, this study proposes a self-powered, flexible, and one-stop implantable triboelectric active sensor (iTEAS) that can provide continuous monitoring of multiple physiological and pathological signs. As demonstrated in human-scale animals, the device can monitor heart rates, reaching an accuracy of ~99%. Cardiac arrhythmias such as atrial fibrillation and ventricular premature contraction can be detected in real-time. Furthermore, a novel method of monitoring respiratory rates and phases is established by analyzing variations of the output peaks of the iTEAS. Blood pressure can be independently estimated and the velocity of blood flow calculated with the aid of a separate arterial pressure catheter. With the core−shell packaging strategy, monitoring functionality remains excellent during 72 h after closure of the chest. The in vivo biocompatibility of the device is examined after 2 weeks of implantation, proving suitability for practical use. As a multifunctional biomedical monitor that is exempt from needing an external power supply, the proposed iTEAS holds great potential in the future of the healthcare industry.

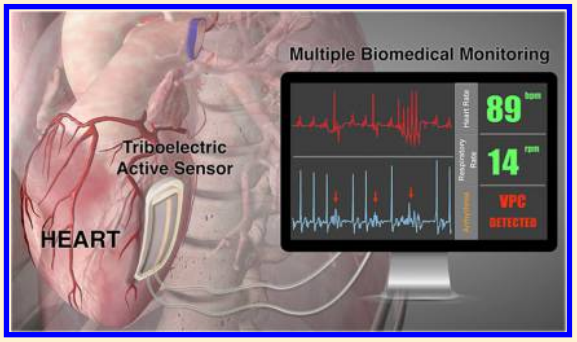

KEYWORDS: *Active sensor, triboelectric nanogenerator, energy harvesting, biomedical monitoring, medical implants, biocompatibility*

Physiological and pathological parameters, such as heart rhythm, respiratory rate, and blood pressure, are major concerns in clinical practice. The absence of the timely detection of sudden changes in vital signs often results in life-threatening conditions and even mortality in a short term. For inpatients, intermittent measurement of the physiological variables could leave out transient or silent symptoms, thus leading to misunderstanding involved in illness evaluations. Moreover, the use of external bulk-size recorders over a long period of time has been hampered by discomfort, complexity, and inadequate patient compliance.[1] The emergence of implantable monitoring devices provides a continuous, stable, and real-time solution, which is critically needed for prompt and reliable diagnosis and intervention for patients with urgent or severe diseases.[2−5] For instance, implantable cardiac monitors (ICMs) could identify potential arrhythmic origins for transitory symptoms such as unexplained syncope or palpitations.[6,7] The application of implantable blood pressure monitors could provide early diagnosis of health problems, accurate assessment of drug efficacy, and reduction of healthcare cost.[8−11] In contrast to wearable biomedical monitoring systems, implantable counterparts bring about a continuous monitoring function of high fidelity and accuracy without activity limitations and artifacts caused by the patient's movement.[12−14]

Owing to unremitting efforts of the medical and engineering communities, implantable monitoring devices experienced a rapid progress in recent years.[15,16] However, heavy reliance upon power supplied by traditional electrochemical batteries limits the operation lifetimes of these devices and therefore constrains the implementation of real-time or continuous biomedical monitoring.[17−20] For example, the new-generation ICMs only have a functioning lifespan of around 36 months.[6] Depleted batteries have to be periodically replaced by surgical procedures that would substantially heighten the morbidity and mortality of patients and increase healthcare financial

Received: May 14, 2016
Revised: August 12, 2016

DOI: 10.1021/acs.nanolett.6b01968
Nano Lett. XXXX, XXX, XXX−XXX

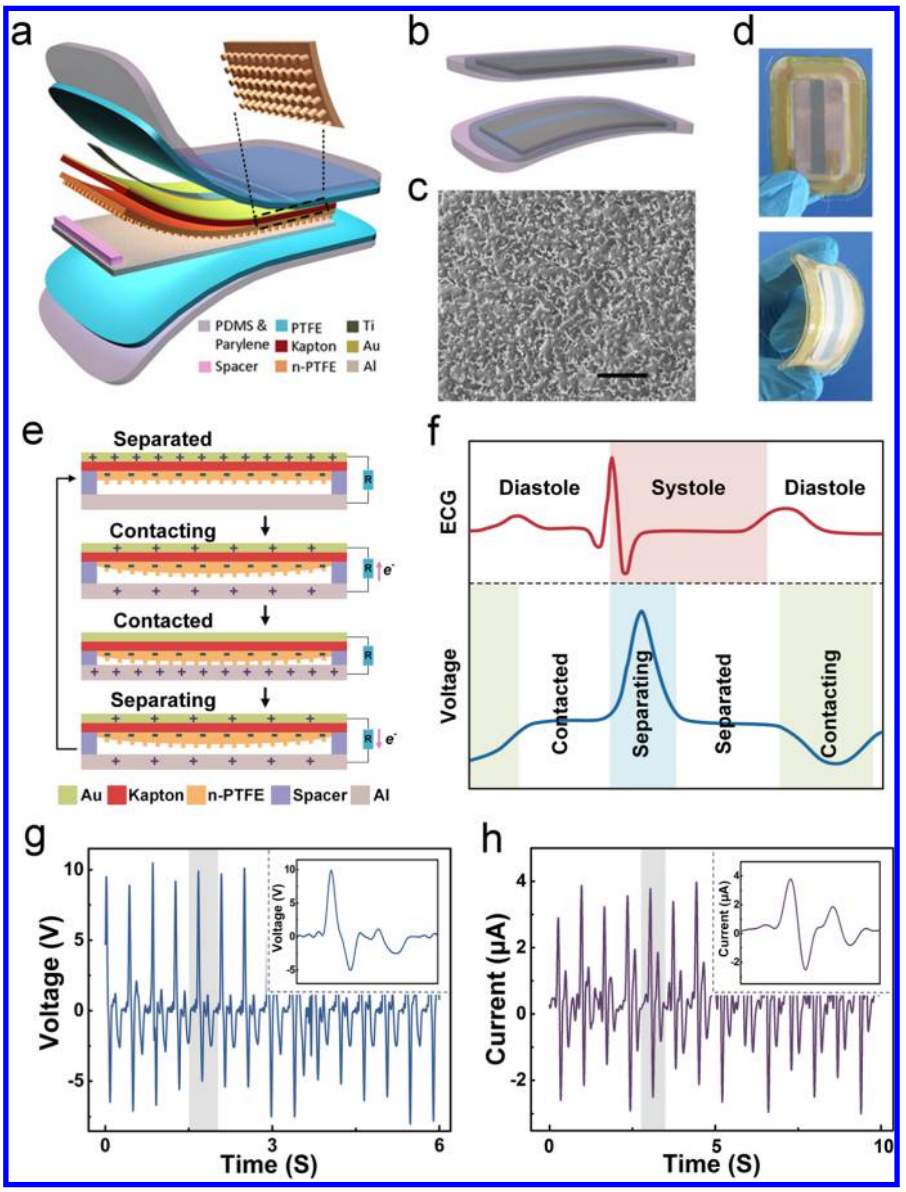

Figure 1. (a) Exploded-view illustration of the structure. (b) Schematic drawings of the iTEAS in original and bending states. (c) SEM image of nanoscale feature of n-PTFE triboelectric layer on elastic Kapton substrate. Scale bar: 5 μm. (d) Photograph of the flexible fabricated nanogenerator. (e) Schematic proposed mechanisms of the device working in a vertical contact-separation mode. (f) Schematic correspondence between voltage output of the iTEAS and different phases of heart motion indicated by ECG. Typical in vivo (g) V_{OC} and (h) I_{SC} of the implanted device. Magnified views of highlighted regions are shown in the inserted figures.

burdens.[21−23] For the minimization of power consumption and the extension of battery life, one approach is to use circuitry that turns the system on for 10 s every 5 min, in essence creating a "sleeping mode" for the devices.[24] However, these solutions are not satisfying, and therefore, a truly continuous and real-time monitoring function is not realized yet.[25]

Recently, a broad spectrum of investigations emerged that focused on harvesting mechanical energy in living environments to replace batteries. Our previous study has demonstrated that the intracorporeal biomechanical energy could be scavenged and converted into electric power.[26−28] However, implantation of both the energy harvester and a medical monitor would occupy more space inside the human body and complicate the surgical procedure, which leads us to believe that a one-stop device will be an ideal solution. Interestingly, we further noticed that abundant biomedical information was contained in the electrical outputs of an implanted nanogenerator. Enlightened by this finding, we inspected the relationship between vital signs and output signals and explored the possibilities of applying implantable nanogenerators to biomedical monitoring.

In this work, we, for the first time, propose a self-powered and multifunctional implantable triboelectric active sensor (iTEAS), which can provide accurate, continuous, and real-time monitoring of multiple physiological and pathological signs. The flexible iTEAS is implanted into the pericardial sac of living swine and fixed to the pericardium. In responding to the heartbeat and breathing, an electric output with an open-circuit voltage (V_{OC}) of ~10 V and a short-circuit current (I_{SC}) of ~4 μA can be yielded, showing a robust self-generated capability and exempting the necessity of an onboard battery. The integration of nanostructured triboelectric layers and pliable encapsulating materials enable the proposed biomedical sensor to detect tiny changes of motions of circumferential organs. As

DOI: 10.1021/acs.nanolett.6b01968
Nano Lett. XXXX, XXX, XXX−XXX

demonstrated in human-scale animals, the device can monitor the heart and respiratory rate, detect life-threatening arrhythmia, and estimate the pressure and the velocity of blood flow with aid of an arterial pressure catheter. With a novel core−shell packaging strategy, the in vivo sensing accuracy and biocompatibility of the device are respectively examined upon 72 h and 2 weeks after closure of chest, suggesting the suitability for practical use.

Results and Discussion. The as-fabricated iTEAS was composed of triboelectric layers, electrodes, and spacers, which were encapsulated with multilayer biocompatible materials, as presented in Figure 1a,b. A nanostructured polytetrafluoroethylene (n-PTFE, 50 μm) thin film was employed as one triboelectric layer and fixed on a Kapton (polyimide) film (150 μm), which served as a substrate for its excellent elasticity and strength. An ultrathin Au layer (50 nm) was deposited on the back side of the Kapton film to form one of the electrodes. Al film (100 μm) was used as both another triboelectric layer and electrode. In addition, it is worth noting that the spacers combined with an elastic titanium strip were integrated on Kapton film to guarantee the contact and separation of triboelectric layers more effectively. Figure 1c shows scanning electron microscopy images of the n-PTFE thin film, which was surface-morphologically modified by dry-etching to create nanoscale features to enhance the surface triboelectric charge density. A core−shell encapsulating strategy was applied to achieve the hermetic, biocompatible, and flexible packaging. PTFE, which has a wide application in medical implants, was used as the first-layer encapsulation material. A flexible PDMS layer was then deployed by spin-coating to enhance the leakproof characteristics. To further increase the stability of the device and avoid potential erosion in the humid and corrosive in vivo environment, a Parylene film was deposited to form a high-density and hole-free coating layer. More details can be found in the Experimental Methods section in the Supporting Information.

Mechanical robustness needs to be assured for long-term in vivo application confronting circumferential extrusion and moisture, while flexibility is required in case of damage to the brittle tissues or compromising of the function of internal organs. Trade-off were made by using this core−shell packaging technique. Mechanical elasticity of the final assembled self-powered active sensor is exhibited in Figure 1d, with a total dimension of 30 × 20 × 1 mm^3. The thickness was strictly controlled to be pliable enough to closely fit the nonplanar surfaces of organs and maintain sensitivity in response to biomechanical motions. The in vitro output performance was examined by a linear motor with periodical mechanical triggering. The V_{OC} and I_{SC} reached ∼75 V and ∼12 μA, respectively, demonstrating considerable self-powered ability (Figure S1a,b).

The working principle of the iTEAS is illustrated in Figure 1e,f. In brief, the triboelectric layers separated and contacted along with the contraction and relaxation of the heart, thus outputting electric signals continuously through the coupling of contact electrification and electrostatic induction. Specifically, the n-PTFE layer was brought into vertical contact with the Al layer during the diastole of the heart, and the electrons were injected from the Al layer into n-PTFE due to the difference in triboelectric series, resulting in a positively charged Al layer and negatively charged n-PTFE. The triboelectric layers contacted when the heart was fully dilated, with positive charges on the Au electrode being screened and the same amount of inductive charges presenting on the Al layer. During the systole of the heart, the n-PTFE separated from the Al layer, and the electrons flowed from the Au electrode to the Al layer. When the heart fully contracted and the triboelectric layers were separated, positive charges on the Al layer were completely screened, and the same amount of inductive charges were presented on Au electrode. Electrons were driven to flow through the external circuit with the dilating and contracting of the heart, thus contributing to cyclic alternating electric output signals.

To simulate the internal environment of human body, a large-scale animal model was deployed for in vivo investigations. Adult Yorkshire pigs (male, 30 kg) were handled by strictly conforming to the "Shanghai Administration Rule of Laboratory Animal" and the Institutional Animal Care and Use Committee (IACUC) approved protocol of the Animal Care Center at the Second Military Medical University. Briefly, the animal was anesthetized with an injection of ketamine (8 mg/kg, intramuscularly (IM)) followed by propofol (1 mg/kg, intravenously (IV)) and then intratracheally intubated and ventilated in a rate of 12 cycles per minute (5 s per cycle). Anesthesia was maintained with 1.0% isoflurane. A midline sternotomy was made on the chest of each of the swine for the implantation of our devices, providing a broad operative field for testing. In consideration of the size and thickness of the sensor (3 cm × 2 cm × 0.1 cm), minimally invasive techniques including intercostal mini-thoracotomy and video-assisted thoracoscopic surgery (VATS) would be feasible in future clinical applications, allowing faster recovery and less scarring.

The iTEAS was implanted into the pericardial sac between the epicardium and pericardium and then affixed to the pericardium, with one stitch used at each corner of the device (Figure S2a). This anchoring method avoided injuries to the myocardium, reduced the risk of bleeding on account of the limited blood vessels on the pericardium, and minimized the disturbance on cardiac motions. Comparative anchoring alternatives, such as fixing onto the epicardium (as previously reported by Rogers' group),[19] optimized output performances by maintaining conformal contact between the epicardium and piezoelectric energy harvesters. However, this was not necessary in our study because it was the rapid vertical contact and separation between the heart and the triboelectric device that efficiently generated the electrical signals. After the implantation and fixation, the pericardium was sutured to achieve complete contact of the iTEAS with the epicardium during cardiac relaxation (Figure S2b). Lead wires, protruding the chest wall, were used to connect the device and a multichannel data acquisition (DAQ) system. The self-powered ability of the active sensor was assessed by the in vivo output performance of V_{OC} and I_{SC}, with no signal conditioning circuit involved, which could reach to 10 V and 4 μA, respectively (Figure 1g,h). Although the in vivo electrical outputs were lower than those of former in vitro tests based on a larger extent of mechanical deformation induced by the external linear motor, it was still higher than at least a majority of previously reported devices for intracorporeal energy harvesting.[18,19,26,27]

Because the electric outputs of the device were transduced from biomechanical energy generated by motions of internal organs, the outputs carry abundant information on biomedical signals. Thus, we proposed that the sensory characteristics of iTEAS could be used for self-powered biomedical monitoring. First, we focused on the relationship between output signals of the iTEAS and fundamental cardiac parameters, including heart

DOI: 10.1021/acs.nanolett.6b01968
Nano Lett. XXXX, XXX, XXX−XXX

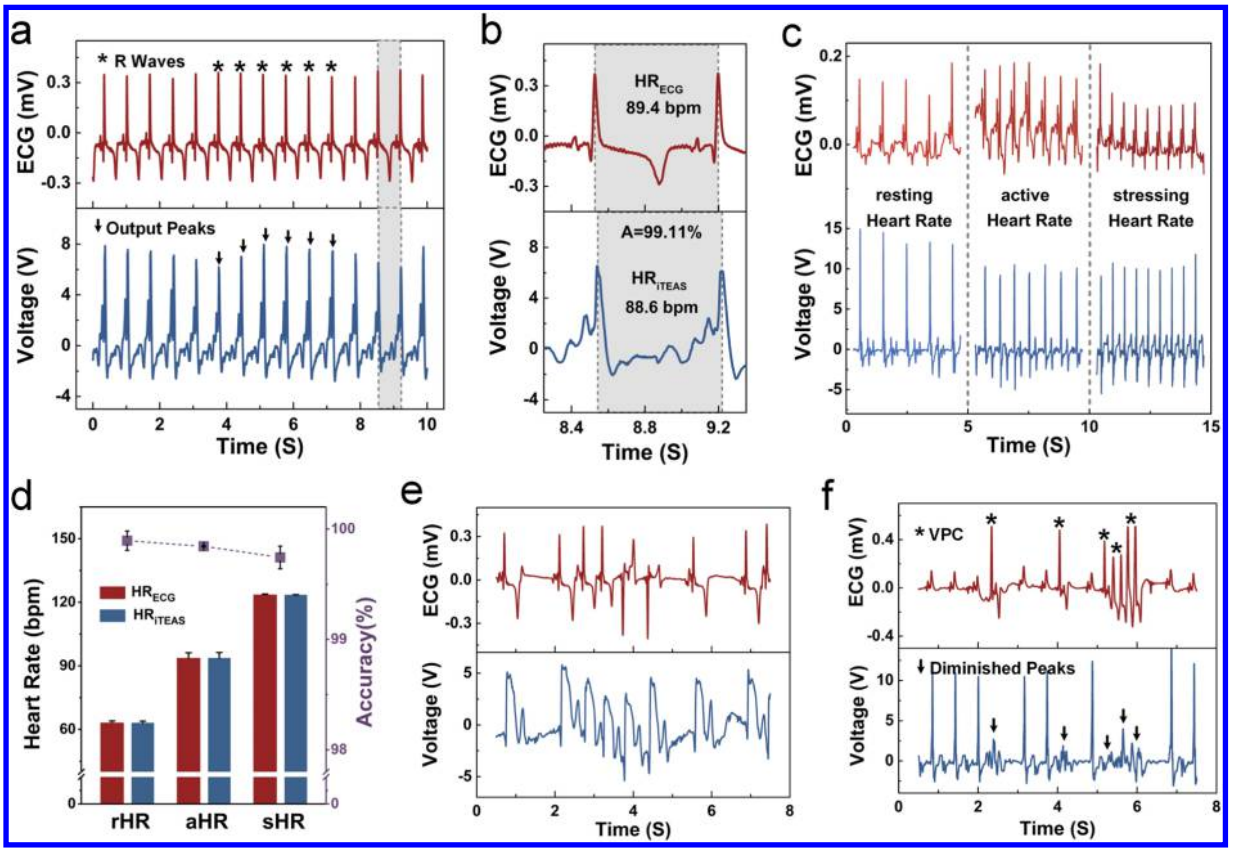

Figure 2. (a) R waves of ECG (asterisks) absolutely corresponded to peaks of voltage output of the iTEAS (arrows). (b) The highlighted region represented time intervals between two enlarged contiguous pairs of the R wave and output voltage. Instant heart rates were calculated to be 89.4 and 88.6 beats per minute (bpm), achieving an accuracy (A) of 99.11%. (c) The consistency between R waves and voltage peaks remained under resting (~60 bpm, rHR), active (~90 bpm, aHR), and stressed (~120 bpm, sHR) conditions. (d) Further analysis of HRs under different states using continuous intervals (n = 6). (e) R−R intervals were unequal between each other but consistent with corresponding peak−peak intervals in an atrial fibrillation porcine model. (f) Ectopic R waves (asterisks) in representative ECG indicating ventricular premature contraction (VPC) corresponded to diminished waveforms (arrows) of the device. All error bars indicate ± sd.

rate (HR) and rhythm. Here, the electrocardiogram (ECG) was selected as the reference standard for its accuracy and reliability in tracking simple heart rate and diagnosis of complex arrhythmias.[29,30] Probes fixed on the skin of the swine were connected to the DAQ system to record ECG results. As depicted in Figure 2a, the peak waves of voltage output are highly synchronous to corresponding R waves in ECGs, which are widely perceived as signs of heartbeats. The time interval between two consecutive QRS complexes, which is conventionally represented by the time between two neighboring R waves, can be used to calculate instantaneous heart rate under physiological conditions. Therefore, HR can be obtained with the following formula:

$$\text{HR (beat per minute)} = 60/\text{p−p interval} \quad (1)$$

where the p−p interval is the time between two consecutive peaks of output V_{OC} or R waves in the ECG. It is worth noting that there occur some small waves between two prominent peaks constantly. These relatively tiny waves are probably raised by the nonsynchronous contraction of different parts of heart, pulsatile coronary arteries on the rough and nonplanar surface of the heart, or oscillation of the heart as a result of turbulent blood flow. They are not stable and could be easily influenced by changing physiological state of the heart and relative position of the implanted device. Therefore, the tiny waves were ignored as noise signals during analysis of the output signals of the proposed sensor. A unified standard to distinguish the P−P intervals were settled: (1) connection of lead wire probes (positive or negative) was marked and fixed, which ensured the consistency of the general directions of data in different experiments or time points; and (2) only peaks of positive and prominent waves in the output voltages were chosen during analysis of the heart rate monitoring function of the device. Our further inspection showed that a high consistency was achieved in HR_{ECG} (HR measured by ECG) and HR_{iTEAS} (HR measured by the iTEAS), as shown in Figure 2b. To quantitatively assess monitoring properties of heart rate, the accuracy (A) of the HR monitoring was defined as the degree of closeness of HR_{iTEAS} to HR_{ECG}, and it could be expressed as

$$A = (1 - |HR_{iTEAS} - HR_{ECG}|/HR_{ECG}) \times 100\% \quad (2)$$

As a result, a high accuracy of ~99% was achieved in the present study, demonstrating an accurate HR monitoring function of the device for normal and regular heartbeats.

Heart rates may vary significantly under different physiological and pathological states. We then tracked performances of the iTEAS under orderly altered heart rates by administrating epinephrine (0.1 mg/mL, IV) and amiodarone (2 mg/mL, IV), which can elevate and reduce HRs, respectively. The synchronicity in peak voltages and R waves remained under resting (~60 beats per minute (bpm)), active

DOI: 10.1021/acs.nanolett.6b01968
Nano Lett. XXXX, XXX, XXX−XXX

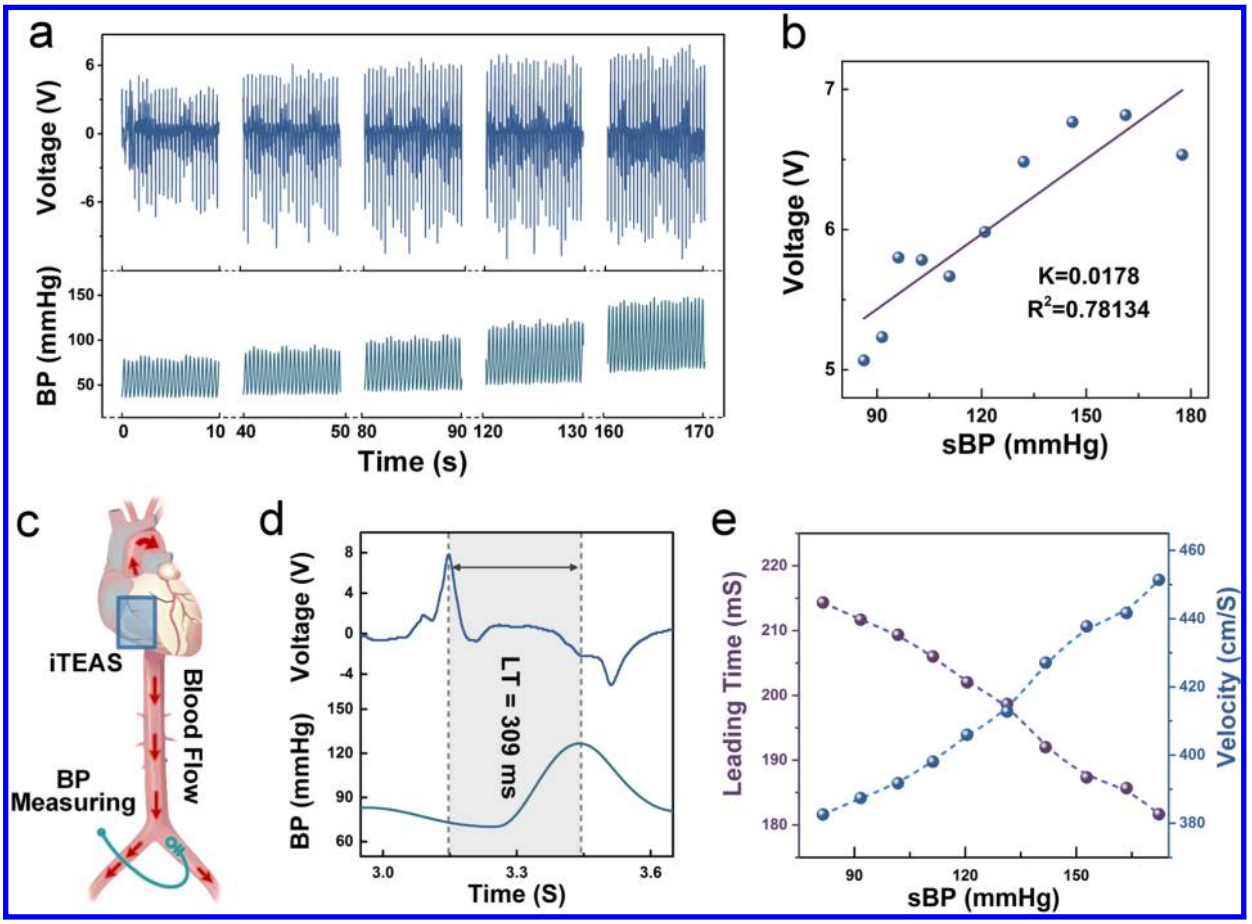

Figure 3. (a) Output of the iTEAS increased along with the blood pressure (BP). (b) Linear correlation between voltage outputs and systolic BP (sBP). Blue points represent mean values of six consecutive peaks, randomly selected every ~20 s. The purple line corresponds to the linear fitting function; *K*, slope of the function; R^2, adjusted R square. (c) Schematic diagram illustrating the mechanisms for monitoring the velocity of blood flow. Red arrows represent the direction of blood flow. (d) Time interval (leading time, LT, shown in highlighted region) between the peaks of the two corresponding waveforms. (e) The leading time decreased and the velocity of blood flow increased along with the elevation of BP. Purple points represents the mean values of three consecutive leading times randomly selected under different sBPs. Blue points represent the mean velocity of blood flow calculated according to the corresponding leading time.

(~90 bpm), and stressed (~120 bpm) states (Figure 2c). In addition, we observed a slightly decreased output voltage during the transition from the resting to the active state. This was partially due to shortened periods of ventricular dilation under increased HRs allowing less blood to flow into ventricles, giving rise to a smaller degree of cardiac relaxation and following the contact of two triboelectric layers. Furthermore, the consistency between HR_{ECG} and HR_{iTEAS} was stable and the accuracy remained high under different physiological states, showing excellent stability and reliability, as illustrated in Figure 2d.

Cardiac arrhythmia with irregular rhythms of heartbeats contributes to significant morbidity and mortality in patients with cardiovascular problems.[31,32] As a distinctive approach different from traditional diagnostic tools such as ECG and Höltor monitor, which cannot provide continuous examination, we tried to detect the arrhythmia through the monitoring of heart motion. Atrial fibrillation (AF) and ventricular premature contraction (VPC), respectively representing supraventricular and ventricular arrhythmia, were opted to demonstrate the monitoring function for arrhythmia of the iTEAS. In an aconitine-induced AF porcine model[33,34] with all R−R intervals unequal in ECG, there was the onset of declined peak waves in output voltage and unequal p−p intervals, which were one-to-one mappings to the unequal R−R intervals (Figure 2e). This result demonstrated the capacity of the iTEAS for detection of AF and timely diagnosis of paroxysmal atrial fibrillation (PAF), which was thought to be an early stage of AF and frequently asymptomatic, exposing patients to the risk of stroke and thromboembolism. Similar results were obtained when VPC was induced by stimulating the ventricle with an external cardiac pacemaker, which was set to 50 bpm in enforce mode (Figure 2f). It is worth noting that the ectopic R waves of VPC, which represent abnormal ventricular contractions, corresponded exactly to the evidently diminished output waves. This behavior suggests that the output performance of the iTEAS is closely associated with the potency and coordination of the cardiac contraction and relaxation, which exhibits potential applications in alerting life-threatening heart attack and ventricular fibrillations.

An arterial pressure catheter was placed in the right femoral artery and connected to the DAQ system through a commercialized transducer widely used in clinical practice. The peak output voltage of the iTEAS increased along with the blood pressure (BP) after an infusion of epinephrine (Figure 3a). The peak voltage decreased accordingly when the BP went down (data not shown). To minimize the interference of respiratory movement on the voltage and blood pressure, a

DOI: 10.1021/acs.nanolett.6b01968
Nano Lett. XXXX, XXX, XXX−XXX

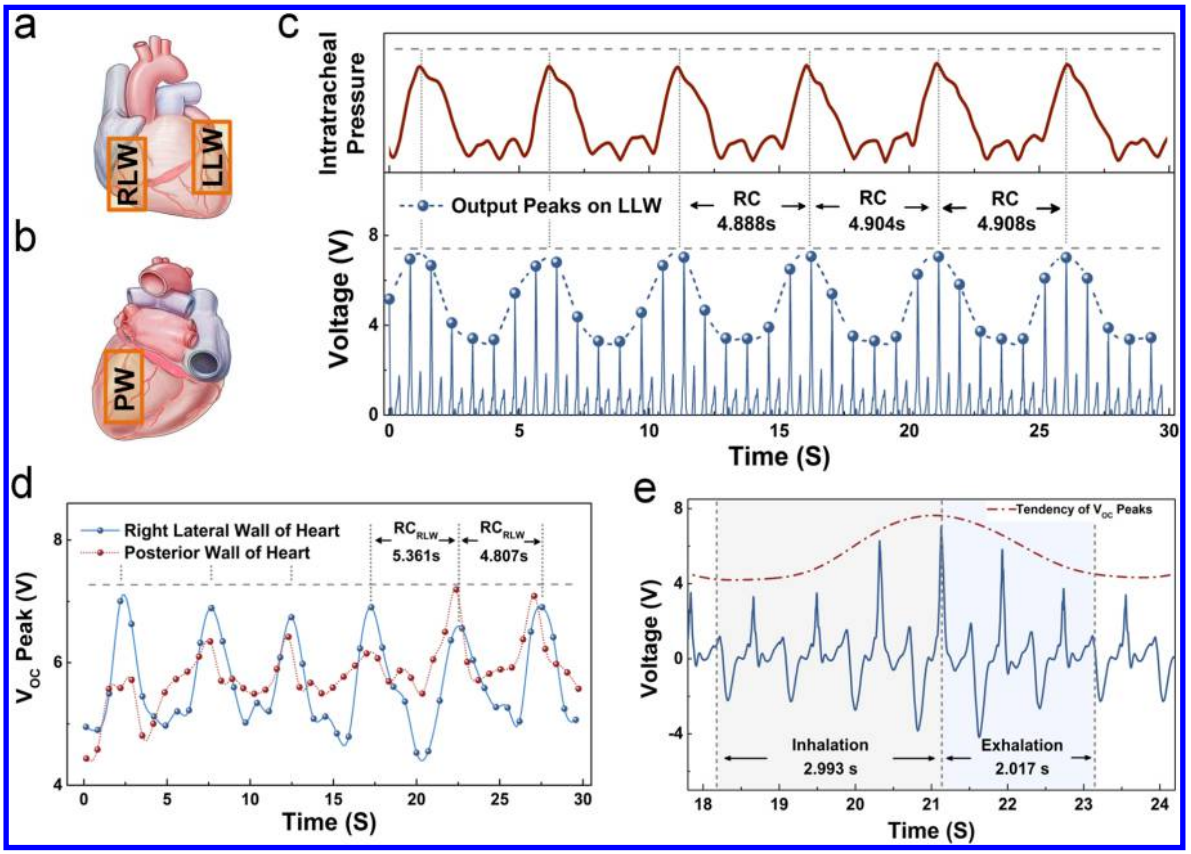

Figure 4. (a) Anterior and (b) posterior views of the heart schematically illustrating three selected implanting sites: the left lateral wall (LLW), right lateral wall (RLW), and posterior wall (PW) of the heart. (c) The peaks of output voltage fluctuated periodically and stably when the iTEAS was anchored over the LLW. Typical time intervals between two neighboring maximal peaks were measured to be ~5s. Blue solid-line curves represent positive waveforms of the output voltage. Blue points stand for the peaks of output voltage. (d) Output peaks of the device over the RLW showed fine but slightly less stable cyclic fluctuations, while output peaks varied irregularly when the iTEAS was placed beneath the PW of the heart. (e) Output peaks increased from ~4.8 to ~6.3 V during the process of inhalation and decreased during the process of exhalation, indicating different respiratory phases. The red line indicates the tendency of variations of output amplitudes.

detailed examination of the relationship between the two involved averaging values of six consecutive peaks was made. Although there is a correlation between the output voltage and systolic blood pressure (sBP) with a sensitivity of 17.8 mV/mmHg, the linearity is not strong ($R^2 = 0.78$) (Figure 3b). This can be explained by the fact that the sBP is not only related to the heart but also depends on several other physiological parameters, such as blood volume, vascular resistance, and elasticity of the arterial wall. Further inspections revealed that the output voltage waves were synchronous but slightly precedent to corresponding BP waves (Figure S3). As schematically illustrated in Figure 3c, the peak voltage appears when the blood is pumping out from the heart, and the recorded BP elevates to the culmination (sBP) when the blood flows through the femoral artery; thus a leading time (LT) exists between two corresponding peaks (Figure 3d). Therefore, the average velocity of blood flow can be calculated as follows:

$$V_{avg} = S/LT \quad (3)$$

Here, V_{avg} is an average velocity of blood flow, S is the length from heart to femoral artery, and LT is the measured leading time. Further study under different sBPs indicated that the velocity of blood flow increased and the leading time reduced when the sBP was elevated, as shown in Figure 3e.

Respiratory rate (RR) presents another vital sign that is valuable for assessing the function of the respiratory system and can also be influenced by a broad spectrum of diseases.[35,36] Traditional methods for RR measurement, including visual observation, acoustic sensing, and impendence pneumography, are time-consuming, costly, or overly sensitive to artifacts brought on by the movements of patients.[37−39] Along with our aforementioned in vivo study, we observed an interesting phenomenon that the magnitude of output voltage was significantly influenced by respiratory motion, characterized by cyclic fluctuations of voltage peaks. Hence, we postulated that iTEAS could be utilized to monitor respiration. In consideration of the influence by the motion of lungs, three sites of implantation were selected to evaluate the monitoring function for respiration: left lateral wall (LLW), right lateral wall (RLW), and posterior wall (PW) of heart (Figure 4a,b). Peak output voltages of the iTEAS at LLW and RLW, which were adjacent to lungs, presented stable periodical fluctuations along with the respiration (Figure 4c,d). Specifically, the time intervals between two neighboring maximal peaks was ~5 s, indicating a respiratory rate of 12 cycles per minute (cpm), which was consistent to the ventilating rate of 12 cpm controlled by the artificial respirator. The intratracheal pressure plot, which can roughly indicate the process and cycles of respiration, was acquired from the artificial ventilator and temporally calibrated with the voltage waveforms. In contrast,

DOI: 10.1021/acs.nanolett.6b01968
Nano Lett. XXXX, XXX, XXX−XXX

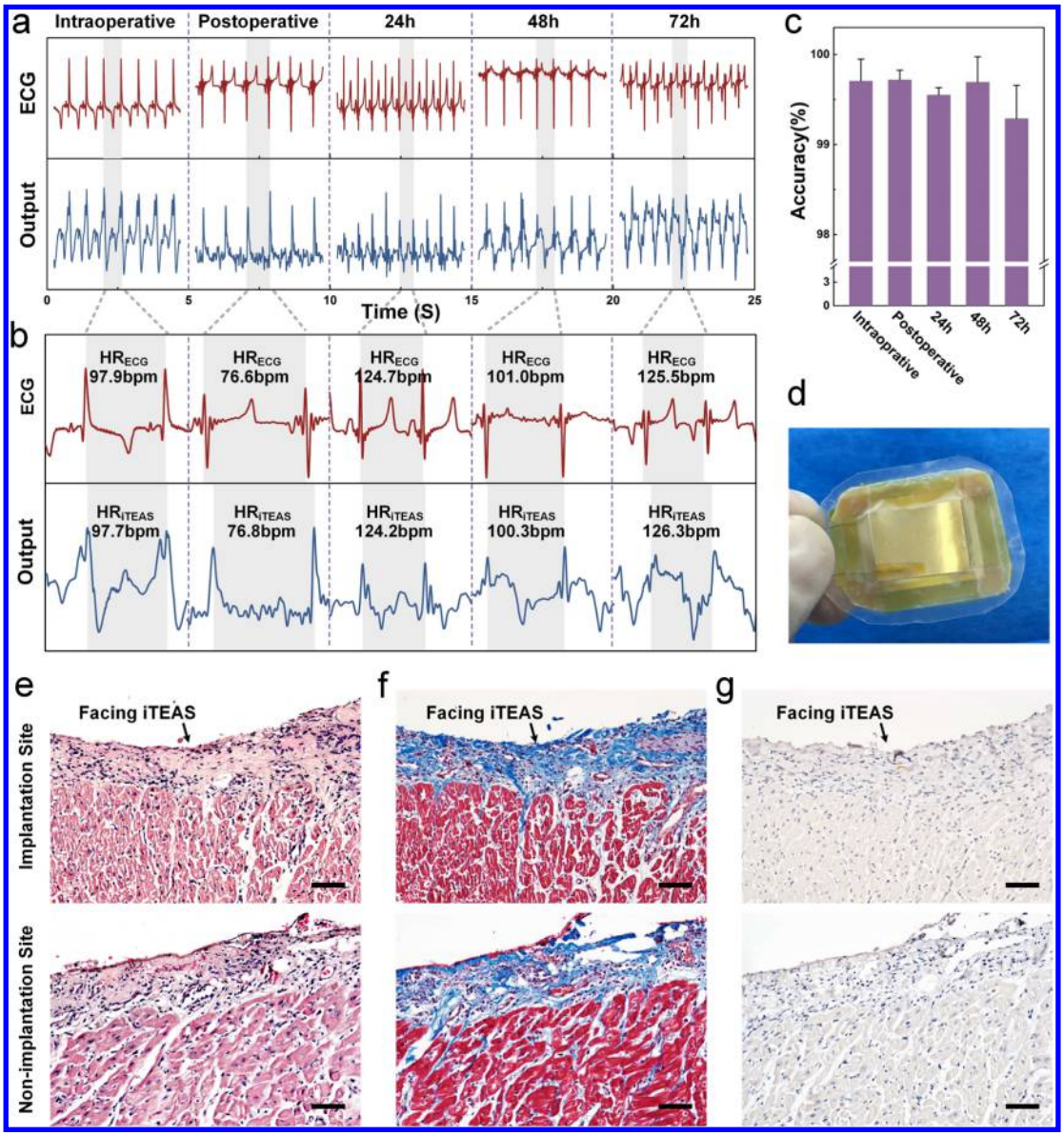

Figure 5. (a) Synchronicity between ECG and output voltage maintained stability for up to 72 h after implantation. Enlarged view of highlighted region was shown in (b). Instant HR_{iTEAS} values remained close to instant HR_{ECG} values during surgical implantation (intraoperative); immediately after closing the chest (postoperative); and 24, 48, and 72 h after implantation. (c) The accuracy of HR monitoring remained high (>99%) for up to 72 h after implantation. (d) Photograph of the iTEAS extracted from the porcine pericardial sac after 2 weeks of implantation without detectable corrosion, rupture. or leakage. (e) Hematoxylin−eosin staining showed no obvious infiltration of lymphocytes in the myocardial tissue at the implantation site. (f) Masson's trichrome stain identified no cardiac tissue damage or obvious increase in the extent of inflammatory fibrous hyperplasia at the implantation site. (g) Immunohistochemistry analysis indicates no significant differences of the expression of cleaved-caspase 3 between the tissues of two sites. Scale bars, 50 μm. All error bars indicate ± sd.

the peak output voltage fluctuated unpredictably and irregularly at the position of PW (Figure 4d), thus demonstrating that lateral walls of heart are the optimal locations for monitoring respiration. This obviously diminished, and unstable changes of output peaks were attributed to relevantly fixed and complicated environment and disturbance from circumferential organs (major vessels and esophageal) around the posterior wall of heart. Interestingly, as shown in Figure 5c, the relatively small peaks, which laid among prominent peaks, also exhibited a similar periodical fluctuation. However, these small waves are not stable enough to be utilized, and the fluctuations in them are much less obvious than the big ones.

Further inspections into the fluctuations revealed that peak output voltage was associated with different phases of a respiratory cycle (RC). Figure 4e illustrates that output peaks increase from ∼4.8 to ∼6.3 V during the process of inhalation and decrease to the baseline during the process of exhalation. In detail, the time periods of increasing and decreasing stages are respectively 2.99 and 2.02 s, leading to a ratio of ∼1.48, which is fairly close to the inhalation/exhalation ratio (I/E ratio) of 1.5:1 set by the ventilator (data for more respiratory cycles can be found in Table S1). Excellent characteristics of distinguishing RC phases can provide reliable suggestions on the diagnosis of metabolic acid−base disturbances and alerts of urgent and adverse paroxysm in patients with chronic obstructive pulmonary disease (COPD) and asthma. Collectively, these results confirmed the potential of iTEAS to be an accurate self-powered respiratory monitor.

DOI: 10.1021/acs.nanolett.6b01968
Nano Lett. XXXX, XXX, XXX−XXX

In vivo durability is a crucial necessity for practical use of an implantable device in a living body. The interaction with the electrolyte-rich aqueous environment within the body could cause inadvertent shorts or electrical leakage if electronic circuits were exposed. With the help of the core−shell hermetic encapsulation, the iTEAS exhibited the same capabilities in biomedical monitoring function from intraoperation to 72 h after chest closure (Figure 5a). Excellent fatigue properties were demonstrated in vivo after ∼350 000 cycles of separation and contact, showing no significant reduction in sensory characteristics. As shown in Figure 5b, consistency between HR_{ECG} and HR_{iTEAS} maintained postoperatively. Quantified accuracies of heart rate monitoring were calculated to stay at >99% upon 72 h after implantation, proving the favorable in vivo durability of the monitoring function of the device (Figure 5c).

Any application inside the human body will require the reliable assessment of biocompatibility and the absence of biotoxicity. Because numerous in cellulo tests were performed in previous studies[40−42] to exclude potential adverse effects of the encapsulating materials on adhesion, growth, and viability of cells, we opted to in vivo examine the influences on adjacent tissues of the circumferential organ. After 2 weeks of implantation, the pig was anesthetized and the iTEAS extracted from the pericardial sac. As expected, the encapsulation layers were intact, and no corrosion or rupture was observed, indicating integrity in the complicated internal environment (Figure 5d). Next, the myocardium tissues at the implantation site and the relatively distal site were obtained for histological study. Hematoxylin and eosin (H&E) staining shows no detectable infiltration of lymphocytes in both sites (Figure 5e), prompting the conclusion that neither humoral nor cellular rejection to the device occurred in myocardium from the implantation site. Masson's trichrome stain was applied, which determined no significant difference between the two sites on the extent of cardiac tissue injury and inflammatory fibrous hyperplasia after prolonged implantation (Figure 5f). As shown in Figure 5g, no apoptosis is noticeable in both samples by immunohistochemical labeling of anticleaved caspase-3 antibody, which is a widely used marker for apoptotic cell death.

In comparison to the biomedical monitor at the body surface, i.e., wearable devices, there are many challenges existing for implantable alternatives. First, the in vivo environment is filled with bodily fluid, which will significantly affect the performance of the device if it leaks into the inner structure. Thus, hermetic packaging has to be guaranteed. Second, the biocompatibility of packaging materials is demanded for in vivo use. Third, the thickness of the encapsulation layer needs to be strictly controlled to maintain the sensitivity of medical implants in responding to biomechanical motions. Finally, the flexibility is required in case of damage to the brittle tissue or compromising of the function of organs inside the body. In the present work, the active structure was encapsulated with compound biocompatible materials in a core−shell structure. PTFE was used for its excellent strength, a PDMS layer was deployed to enhance the leakproof characteristics, and Parylene film was deposited to form a high-density and hole-free coating layer to circumvent potential erosion for in vivo environment.[43] All layers were deployed with a microscale thickness to maintain the sensitivity and flexibility for the device. Here, the absence of both corrosions or ruptures in the device and adverse influences on the surrounding tissue demonstrates an excellent bidirectional biocompatibility, which is a requirement for operation in the human body.

A battery-free and fully implantable monitor could provide early detection or even real-time diagnosis, sever the tether to the bulky size of an onboard battery, and avoid the necessity of surgical replacement for depleted batteries. As a powerful means of scavenging mechanical energy in the ambient environment, nanogenerators emerged as a promising solution for the power supply of medical monitors. Besides the robust self-powered capability, the excellent flexibility and sensitivity of the iTEAS proposed in this study enable us to extract abundant biomedical information from the output signals. This one-stop solution will significantly reduce surgical risks of patients by simplify the implanting procedure. Via incorporation with an active telemetry, the monitored signals could be wirelessly transmitted to an external device, e.g., smart phones, and therefore, the device could be employed as an ideal component for a wireless body sensor network (WBSN) in future health strategies.

Conclusions. This work presents a novel multifunctional implantable triboelectric active sensor that could provide real-time and continuous monitoring functions for various physiological and pathological signs by sensing the biomechanical motion of intracorporeal organs. With the robust self-powered capability, the proposed device exempts the necessity of onboard battery. The rates of heartbeats and respiration can be precisely monitored and life-threatening arrhythmia detected in a timely fashion. Furthermore, the pressure and velocity of blood flow could be estimated. The core−shell packaging strategy guarantees the in vivo durability and bidirectional biocompatibility of the device, which is a requirement for the practical application in human body. On the basis of the multilayer thin-film structure, the iTEAS obtains ideal flexibility and thickness, which is favorable for implantation into body through a minimally invasive surgical technique. In addition, the in vivo experiments in human-scale animals provide more-valuable and -comparable results for clinical application than do small animals. With the aforementioned advances, this work provides the proof-of-concept demonstration for the next-generation implantable biomedical sensor.

■ ASSOCIATED CONTENT

Supporting Information

The Supporting Information is available free of charge on the ACS Publications website at DOI: 10.1021/acs.nanolett.6b01968.

Additional experimental details including device structure and fabrication, the in vivo study, animal models, and histological evaluation of in vivo biocompatibility. A discussion on the source and management of small waves of voltage outputs. Figures showing the typical open-circuit voltage and the short-circuit current of the iTEAS, device insertion, and the synchronicity between waveforms of output voltage and blood pressure. A table showing the monitoring of respiratory phases and I/E ratio. (PDF)

■ AUTHOR INFORMATION

Corresponding Authors

*Z.L.W. e-mail: zhong.wang@mse.gatech.edu.
*Z.L. e-mail: zli@binn.cas.cn.
*H.Z. e-mail: zhanghao@smmu.edu.cn.

DOI: 10.1021/acs.nanolett.6b01968
Nano Lett. XXXX, XXX, XXX−XXX

Author Contributions

H.Z., Z.L., and Z.L.W. conceived the idea and designed the experiments. Y.M., Q.Z., and Y.L. performed experiments and prepared figures. B.S., Z.L., Y.J., Y.Z., and X.W. designed, fabricated, and tested the devices and analyzed data. X.X. and Z.A. performed animal experiments and performed histological study. Z.X. and Z.L.W. designed experiments and edited the manuscript. The manuscript was written through contributions of all authors. All authors have given approval to the final version of the manuscript. Y.M., Q.Z., and Y.L. contributed equally.

Funding

This work was supported by the "Thousands Talents" program for the pioneer researcher and his innovation team, the National Natural Science Foundation of China (grant nos. 81271707, 81371692, 81370335, 31571006, and 30700157), and the Beijing Talents Fund (2015000021223ZK21).

Notes

The authors declare no competing financial interest.

■ ABBREVIATIONS

iTEAS, implantable triboelectric active sensor; ICMs, implantable cardiac monitors; *n*-PTFE, CC nanostructured polytetrafluoroethylene; V_{OC}, open-circuit voltage; I_{SC}, short-circuit current; VATS, video-assisted thoracoscopic surgery; HR, heart rate; ECG, electrocardiogram; IM, intramuscularly; IV, intravenously; AF, atrial fibrillation; VPC, ventricular premature contraction; PAF, paroxysmal atrial fibrillation; BP, blood pressure; LT, leading time; RR, respiratory rate; LLW, left lateral wall; RLW, right lateral wall; PW, posterior wall; RC, respiratory cycle; *I*/*E* ratio, inhalation-to-exhalation ratio; COPD, chronic obstructive pulmonary disease; WBSN, wireless body sensor network

■ REFERENCES

(1) Zimetbaum, P.; Josephson, M. E. *N. Engl. J. Med.* **1998**, *338* (19), 1369−73.
(2) Chen, L. Y.; Tee, B. C.; Chortos, A. L.; Schwartz, G.; Tse, V.; Lipomi, D. J.; Wong, H. S.; McConnell, M. V.; Bao, Z. *Nat. Commun.* **2014**, *5*, 5028.
(3) Abraham, W. T.; Stough, W. G.; Pina, I. L.; Linde, C.; Borer, J. S.; De Ferrari, G. M.; Mehran, R.; Stein, K. M.; Vincent, A.; Yadav, J. S.; Anker, S. D.; Zannad, F. *Nat. Rev. Cardiol.* **2014**, *11* (10), 576−85.
(4) Ritzema, J.; Melton, I. C.; Richards, A. M.; Crozier, I. G.; Frampton, C.; Doughty, R. N.; Whiting, J.; Kar, S.; Eigler, N.; Krum, H.; Abraham, W. T.; Troughton, R. W. *Circulation* **2007**, *116* (25), 2952−9.
(5) Rozenman, Y.; Schwartz, R. S.; Shah, H.; Parikh, K. H. *J. Am. Coll. Cardiol.* **2007**, *49* (7), 784−9.
(6) Giada, F.; Bertaglia, E.; Reimers, B.; Noventa, D.; Raviele, A. *Pacing and clinical electrophysiology: PACE* **2012**, *35* (9), 1169−78.
(7) Krahn, A. D.; Pickett, R. A.; Sakaguchi, S.; Shaik, N.; Cao, J.; Norman, H. S.; Guerrero, P. *Pacing and clinical electrophysiology: PACE* **2014**, *37* (4), 505−11.
(8) Murphy, O. H.; Bahmanyar, M. R.; Borghi, A.; McLeod, C. N.; Navaratnarajah, M.; Yacoub, M. H.; Toumazou, C. *Biomed. Microdevices* **2013**, *15* (5), 737−49.
(9) Sharma, T.; Aroom, K.; Naik, S.; Gill, B.; Zhang, J. X. *Ann. Biomed. Eng.* **2013**, *41* (4), 744−51.
(10) Schlierf, R.; Horst, U.; Ruhl, M.; Schmitz-Rode, T.; Mokwa, W.; Schnakenberg, U. *J. Micromech. Microeng.* **2007**, *17* (7), S98−S102.
(11) Potkay, J. A. *Biomed. Microdevices* **2008**, *10* (3), 379−92.
(12) Darwish, A.; Hassanien, A. E. *Sensors* **2011**, *11* (6), 5561−95.
(13) Konstantas, D. *Yearbook of Medical Informatics* **2007**, 66−9.
(14) Shults, M. C.; Rhodes, R. K.; Updike, S. J.; Gilligan, B. J.; Reining, W. N. *IEEE Trans. Biomed. Eng.* **1994**, *41* (10), 937−42.
(15) Lau, C. P.; Siu, C. W.; Tse, H. F. *Circulation* **2014**, *129* (7), 811−22.
(16) Beck, H.; Boden, W. E.; Patibandla, S.; Kireyev, D.; Gupta, V.; Campagna, F.; Cain, M. E.; Marine, J. E. *Am. J. Cardiol.* **2010**, *106* (6), 810−818.
(17) Amin Karami, M.; Inman, D. J. *Appl. Phys. Lett.* **2012**, *100* (4), 042901.
(18) Hwang, G. T.; Byun, M.; Jeong, C. K.; Lee, K. J. *Adv. Healthcare Mater.* **2015**, *4* (5), 646−58.
(19) Dagdeviren, C.; Yang, B. D.; Su, Y.; Tran, P. L.; Joe, P.; Anderson, E.; Xia, J.; Doraiswamy, V.; Dehdashti, B.; Feng, X.; Lu, B.; Poston, R.; Khalpey, Z.; Ghaffari, R.; Huang, Y.; Slepian, M. J.; Rogers, J. A. *Proc. Natl. Acad. Sci. U. S. A.* **2014**, *111* (5), 1927−32.
(20) Shi, B.; Zheng, Q.; Jiang, W.; Yan, L.; Wang, X.; Liu, H.; Yao, Y.; Li, Z.; Wang, Z. L. *Adv. Mater.* **2016**, *28*, 846.
(21) Athan, E.; Chu, V. H.; Tattevin, P.; Selton-Suty, C.; Jones, P.; Naber, C.; Miro, J. M.; Ninot, S.; Fernandez-Hidalgo, N.; Durante-Mangoni, E.; Spelman, D.; Hoen, B.; Zupanc, T. L.; Cecchi, E.; Thuny, F.; Hannan, M. M.; Pappas, P.; Henry, M.; Fowler, V. G., Jr.; Crowley, A. L.; Wang, A. *Int. J. Antimicrob. Agents* **2012**, *307* (16), 1727−35.
(22) Greenspon, A. J.; Patel, J. D.; Lau, E.; Ochoa, J. A.; Frisch, D. R.; Ho, R. T.; Pavri, B. B.; Kurtz, S. M. *J. Am. Coll. Cardiol.* **2011**, *58* (10), 1001−6.
(23) Cassagneau, R.; Ploux, S.; Ritter, P.; Jan, E.; Barandon, L.; Deplagne, A.; Clementy, J.; Haissaguerre, M.; Bordachar, P. *Pacing and Clinical Electrophysiology* **2011**, *34* (2), 150−154.
(24) Chua-Chin, W.; Chi-Chun, H.; Jian-Sing, L.; Yan-Jhin, C.; Huang, I. Y.; Chih-Peng, L.; Yung-Chin, L.; Weng-Jeng, W. *IEEE Transactions on Biomedical Circuits and Systems* **2008**, *2* (1), 44−9.
(25) Green, B. B.; Cook, A. J.; Ralston, J. D.; Fishman, P. A.; Catz, S. L.; Carlson, J.; Carrell, D.; Tyll, L.; Larson, E. B.; Thompson, R. S. *JAMA* **2008**, *299* (24), 2857−67.
(26) Zheng, Q.; Shi, B.; Fan, F.; Wang, X.; Yan, L.; Yuan, W.; Wang, S.; Liu, H.; Li, Z.; Wang, Z. L. *Adv. Mater.* **2014**, *26* (33), 5851−6.
(27) Zhang, H.; Zhang, X.-S.; Cheng, X.; Liu, Y.; Han, M.; Xue, X.; Wang, S.; Yang, F.; A S, S.; Zhang, H.; Xu, Z. *Nano Energy* **2015**, *12*, 296−304.
(28) Tang, W.; Tian, J.; Zheng, Q.; Yan, L.; Wang, J.; Li, Z.; Wang, Z. L. *ACS Nano* **2015**, *9* (8), 7867−73.
(29) Phua, C. T.; Lissorgues, G.; Gooi, B. C.; Mercier, B. *Int. J. Biosci., Biochem. Bioinf.* **2012**, 110−116.
(30) Ho, D.; Zhao, X.; Gao, S.; Hong, C.; Vatner, D. E.; Vatner, S. F. *Current protocols in mouse biology* **2011**, *1*, 123−139.
(31) Walsh, J. A., 3rd; Topol, E. J.; Steinhubl, S. R. *Circulation* **2014**, *130* (7), 573−81.
(32) Mozaffarian, D.; Benjamin, E. J.; Go, A. S.; Arnett, D. K.; Blaha, M. J.; Cushman, M.; de Ferranti, S.; Despres, J. P.; Fullerton, H. J.; Howard, V. J.; Huffman, M. D.; Judd, S. E.; Kissela, B. M.; Lackland, D. T.; Lichtman, J. H.; Lisabeth, L. D.; Liu, S.; Mackey, R. H.; Matchar, D. B.; McGuire, D. K.; Mohler, E. R., 3rd; Moy, C. S.; Muntner, P.; Mussolino, M. E.; Nasir, K.; Neumar, R. W.; Nichol, G.; Palaniappan, L.; Pandey, D. K.; Reeves, M. J.; Rodriguez, C. J.; Sorlie, P. D.; Stein, J.; Towfighi, A.; Turan, T. N.; Virani, S. S.; Willey, J. Z.; Woo, D.; Yeh, R. W.; Turner, M. B. *Circulation* **2015**, *131* (4), e29−e322.
(33) Machida, T.; Hashimoto, N.; Kuwahara, I.; Ogino, Y.; Matsuura, J.; Yamamoto, W.; Itano, Y.; Zamma, A.; Matsumoto, R.; Kamon, J.; Kobayashi, T.; Ishiwata, N.; Yamashita, T.; Ogura, T.; Nakaya, H. *Circ.: Arrhythmia Electrophysiol.* **2011**, *4* (1), 94−102.
(34) Hashimoto, N.; Yamashita, T.; Fujikura, N.; Tsuruzoe, N. *Europace: European pacing, arrhythmias, and cardiac electrophysiology: journal of the working groups on cardiac pacing, arrhythmias, and cardiac cellular electrophysiology of the European Society of Cardiology* **2007**, *9* (4), 246−51.
(35) Lazaro, J.; Alcaine, A.; Romero, D.; Gil, E.; Laguna, P.; Pueyo, E.; Bailon, R. *Ann. Biomed. Eng.* **2014**, *42* (10), 2072−83.

DOI: 10.1021/acs.nanolett.6b01968
Nano Lett. XXXX, XXX, XXX−XXX

(36) Meredith, D. J.; Clifton, D.; Charlton, P.; Brooks, J.; Pugh, C. W.; Tarassenko, L. *J. Med. Eng. Technol.* **2012**, *36* (1), 1−7.
(37) Folke, M.; Cernerud, L.; Ekstrom, M.; Hok, B. *Med. Biol. Eng. Comput.* **2003**, *41* (4), 377−83.
(38) Farre, R.; Montserrat, J. M.; Navajas, D. *Eur. Respir. J.* **2004**, *24* (6), 1052−60.
(39) Zhu, X.; Chen, W.; Nemoto, T.; Kanemitsu, Y.; Kitamura, K.; Yamakoshi, K.; Wei, D. *IEEE Trans. Biomed. Eng.* **2006**, *53* (12), 2553−63.
(40) Yue, Z.; Liu, X.; Molino, P. J.; Wallace, G. G. *Biomaterials* **2011**, *32* (21), 4714−24.
(41) Palchesko, R. N.; Zhang, L.; Sun, Y.; Feinberg, A. W. *PLoS One* **2012**, *7* (12), e51499.
(42) Astolfi, L.; Simoni, E.; Martini, A. *Hearing, Balance and Communication* **2015**, *13* (4), 166−174.
(43) Pignatello, R. *Advances in Biomaterials Science and Biomedical Applications* InTech: Rijeka, Croatia, 2013.

DOI: 10.1021/acs.nanolett.6b01968
Nano Lett. XXXX, XXX, XXX−XXX